

# On Cartesian Motions with Singularities Avoidance for Free-floating Space Robots

Kostas Nanos, *Student Member, IEEE* and Evangelos Papadopoulos, *Senior Member, IEEE*

**Abstract.** Free-floating space manipulator systems have spacecraft actuators turned off and exhibit nonholonomic behavior due to angular momentum conservation. Such systems are subject to path dependent Dynamic Singularities (DS) that complicate their path planning. Due to the existence of DS its workspace is restricted. The Cartesian space path planning of free-floating space robots is studied and a novel path planning technique allowing the end-effector to follow a desired path avoiding any DS is proposed. Since the path is predefined, the method yields the appropriate initial system configurations that avoid dynamically singular configurations during the motion. Therefore, it allows effective use of the entire robot workspace. The proposed method is applicable to both planar and spatial systems and it is demonstrated using straight-line paths. The application of the method is illustrated by two examples.

## I. INTRODUCTION

Robotic manipulators are playing important roles in planetary exploration and in tasks on orbit, due to their ability to work in environments that are inaccessible or too risky for humans. On orbit robotic systems, or free-flying space manipulator systems, see Fig. 1, include a thruster equipped satellite base with robotic manipulators mounted on it. Early examples of such systems are the ETS-7 and the Orbital-Express.

To conserve fuel or electric power and to avoid interactions with nearby objects, all base actuators can be turned off. Then, the system operates in a free-floating mode during which, dynamic coupling exists between the manipulator and its base and the spacecraft translates and rotates in response to manipulator motions. This mode of operation is feasible only when no external forces and torques act on the system and when the initial momentum of the system is zero. The effective Cartesian Space path planning of such systems is hindered by Dynamic Singularities (DS) [1]. Hence, the ability to drive a robot end-effector via a desired path and avoiding dynamic singularities is important and is studied here.

Franch et al. used flatness theory to plan trajectories for free-floating systems, [2]. Their method employs a specific system design so that the system is made controllable and linearizable by prolongations. Agrawal et al. extended this method to a three-link spatial space robot, [3]. Nenchev et al. presented the kinematics and momentum equations, focusing on the redundant nature of free-flying systems, [4]. They re-

solved system redundancy using a least squares approach and applied the techniques on tasks with zero system momentum. Tortopidis and Papadopoulos have developed a joint space, polynomial function-based planning methodology, that allows simultaneous manipulator point-to-point and spacecraft attitude control using manipulator actuators only, [5]. Papadopoulos has presented a point-to-point Cartesian space planning method that permits the effective use of a system's reachable workspace avoiding DS, [6]. Xu et al. have proposed a trajectory planning method that uses damped least squares to avoid a DS by deviating the end-effector from its desired path, [7]. Umetani and Yoshida, [8], have developed a resolved motion rate control method based on the Generalized Jacobian matrix. However, the method fails in the presence of DS. Nanos and Papadopoulos have proposed a methodology that determines the workspace volumes and the necessary joint rates where the end-effector can remain fixed despite the presence of angular momentum, [9].

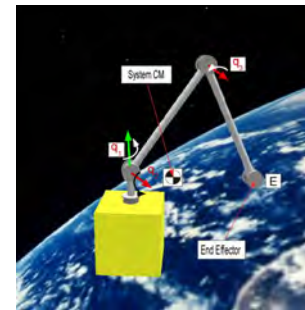


Fig. 1. A free-floating space manipulator system.

In this paper, the path planning of free-floating space robots in Cartesian space is studied. The workspace of such systems is restricted due to the existence of DS and its path planning is complicated. A novel path planning methodology allowing the end-effector to follow a given path avoiding DS is proposed. To follow a predefined path, the method yields the appropriate initial system configurations that avoid dynamically singular configurations during the desired motion, resulting in the effective use of the entire workspace. The proposed method is applied here to planar systems with straight-line paths and is extended to 3-dof spatial systems. Two examples illustrate the application of the methodology.

## II. DYNAMICS OF FREE-FLOATING SPACE MANIPULATORS

A space manipulator system consists of a spacecraft and a manipulator mounted on it, see Fig. 1. When the system is operating in free-floating mode, the spacecraft's attitude control system is turned off. In this mode, no external forces

Kostas Nanos is with the Dept. of Mechanical Engineering, National Technical University of Athens, Greece (e-mail: knanos@mail.ntua.gr).

Evangelos Papadopoulos is with the Dept. of Mechanical Engineering, National Technical University of Athens, Greece (phone: +30-210-772-1440; fax: +30-210-772-1450; e-mail: egpapado@central.ntua.gr).

and torques act on the system, and hence the spacecraft translates and rotates in response to manipulator movements. This section develops briefly the equations of motion of a rigid free-floating spatial system. According to the current practice in space, the manipulator has revolute joints and an open chain kinematic configuration, so that, in a system with an  $N$  degree-of-freedom (dof) manipulator, there will be  $N+6$  dof in total. Under the assumption of no external forces, the system Center of Mass (CM) does not accelerate, and the system linear momentum is constant. With the further assumption of zero initial linear momentum, the system CM remains fixed in inertial space, and the origin,  $O$ , can be chosen to be the system CM, see Fig. 2.

The conservation of angular momentum is written as:

$${}^0\mathbf{D}(\mathbf{q}) {}^0\boldsymbol{\omega}_0 + {}^0\mathbf{D}_q(\mathbf{q})\dot{\mathbf{q}} = \mathbf{R}_0^T(\boldsymbol{\epsilon}, n) \mathbf{h}_{\text{CM}} \quad (1)$$

where  ${}^0\boldsymbol{\omega}_0$  is the spacecraft angular velocity expressed in the spacecraft  $0^{\text{th}}$  frame, the  $N \times 1$  vectors  $\mathbf{q}, \dot{\mathbf{q}}$  represent manipulator joint angles and rates respectively, and  ${}^0\mathbf{D}, {}^0\mathbf{D}_q$  are inertia-type matrices of appropriate dimensions, given in [1]. The  $\mathbf{R}_0(\boldsymbol{\epsilon}, n)$  is the rotation matrix between the spacecraft  $0^{\text{th}}$  and the inertial frame expressed as a function of the spacecraft Euler parameters  $\boldsymbol{\epsilon}, n$ , and  $\mathbf{h}_{\text{CM}}$  is the system initial angular momentum expressed in the inertial frame.

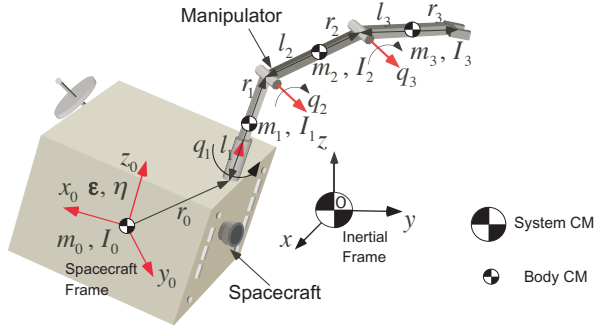


Fig. 2. The spatial free-floating space robot and definition of its parameters.

The end-effector linear velocity is:

$$\dot{\mathbf{r}}_E = \mathbf{R}_0(\boldsymbol{\epsilon}, n) ({}^0\mathbf{J}_{11} {}^0\boldsymbol{\omega}_0 + {}^0\mathbf{J}_{12} \dot{\mathbf{q}}) \quad (2)$$

where the  ${}^0\mathbf{J}_{11}, {}^0\mathbf{J}_{12}$  terms are functions of the system configuration  $\mathbf{q}$  and are given in detail in [1].

It can be shown that the  $N$  equations of motion for a free-floating system have the form, [9]:

$$\mathbf{H}(\mathbf{q})\ddot{\mathbf{q}} + \mathbf{c}_h(\boldsymbol{\epsilon}, n, \mathbf{q}, \dot{\mathbf{q}}, \mathbf{h}_{\text{CM}}) = \boldsymbol{\tau} \quad (3)$$

where  $\mathbf{H}$  is an  $N \times N$  positive definite symmetric matrix, called the reduced system inertia matrix, the vector  $\mathbf{c}_h$  contains the nonlinear Coriolis and centrifugal terms and is a function of the system attitude, configuration, joint rates and angular momentum, and  $\boldsymbol{\tau}$  is the joint torque vector.

### III. PATH PLANNING AND DYNAMIC SINGULARITIES

In this section, we focus on the Cartesian space path planning of a free-floating manipulator whose end-effector has to follow a desired path in prescribed time. The path is defined by the end-effector linear velocity  $\mathbf{v}_E = \dot{\mathbf{r}}_E(t)$ , i.e. the end-effector moves from an initial point to a final one, following

a specific desired path. During system motion, the conservation of angular momentum, given by (1), must be satisfied. Combining (1) and (2) in matrix form, results in the following equation:

$$\mathbf{A} \begin{bmatrix} {}^0\boldsymbol{\omega}_0 \\ \dot{\mathbf{q}} \end{bmatrix} = \begin{bmatrix} \mathbf{R}_0^T & \mathbf{0} \\ \mathbf{0} & \mathbf{R}_0^T \end{bmatrix} \begin{bmatrix} \mathbf{h}_{\text{CM}} \\ \dot{\mathbf{r}}_E \end{bmatrix} \quad (4)$$

where the  $6 \times (N+3)$  matrix  $\mathbf{A}$  is given by:

$$\mathbf{A} = \begin{bmatrix} {}^0\mathbf{D} & {}^0\mathbf{D}_q \\ {}^0\mathbf{J}_{11} & {}^0\mathbf{J}_{12} \end{bmatrix} \quad (5)$$

Given  $\dot{\mathbf{r}}_E(t)$  and  $\mathbf{h}_{\text{CM}}$ , (4) yields the required joints rates and the spacecraft angular velocity that will result. Eq. (4) has at least one solution, if  $N \geq 3$ . So the minimum number of manipulator joints of a spatial system, for a given spatial trajectory  $\dot{\mathbf{r}}_E(t)$ , is three. Note that in planar systems this number reduces to two.

When  $N = 3$ , (4) has only one solution, if and only if, [9]:

$$\det(\mathbf{S}) \neq 0 \quad (6)$$

where  $\mathbf{S}$ , called the Generalized Jacobian in [8], is given by,

$$\mathbf{S} = -{}^0\mathbf{J}_{11} {}^0\mathbf{D}^{-1} {}^0\mathbf{D}_q + {}^0\mathbf{J}_{12} \quad (7)$$

The equation  $\det(\mathbf{S})=0$  defines the DS in the joint space and when it holds, the system Jacobian loses its full rank. Due to the DS, the manipulator reachable workspace is divided in two regions. In the first, called the Path Independent Workspace (PIW), no dynamic singularities can occur while in the second, called the Path Dependent Workspace (PDW), the manipulator may become singular depending on the end-effector path taken to reach a point, [1]. The PIW and PDW for the two-dof planar system in Fig. 3 are shown in Fig. 4a.

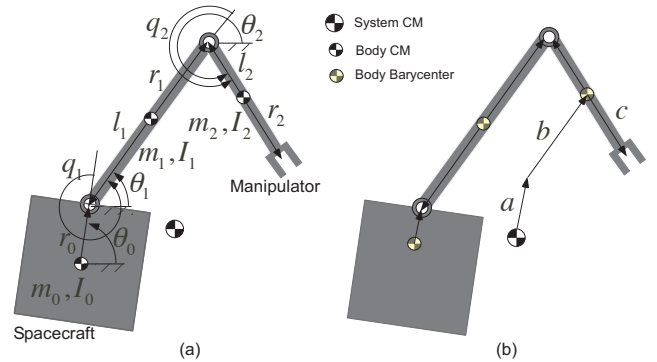


Fig. 3. (a) Definition of system mass properties and configuration parameters, (b) System barycentric vectors  $\mathbf{a}$ ,  $\mathbf{b}$ , and  $\mathbf{c}$ .

If (6) is satisfied, then during the motion of the end-effector, the spacecraft angular velocity expressed in the spacecraft  $0^{\text{th}}$  frame, will be:

$${}^0\boldsymbol{\omega}_0 = [{}^0\mathbf{D}^{-1} + {}^0\mathbf{D}^{-1} {}^0\mathbf{D}_q \mathbf{S}^{-1} {}^0\mathbf{J}_{11} {}^0\mathbf{D}^{-1}] \mathbf{R}_0^T \mathbf{h}_{\text{CM}} - {}^0\mathbf{D}^{-1} {}^0\mathbf{D}_q \mathbf{S}^{-1} \mathbf{R}_0^T \dot{\mathbf{r}}_E \quad (8a)$$

while the vector of the joint rates will be given by:

$$\dot{\mathbf{q}} = -\mathbf{S}^{-1} {}^0\mathbf{J}_{11} {}^0\mathbf{D}^{-1} \mathbf{R}_0^T \mathbf{h}_{\text{CM}} + \mathbf{S}^{-1} \mathbf{R}_0^T \dot{\mathbf{r}}_E \quad (8b)$$

As shown by (8), the configuration rates and the spacecraft angular velocity are proportional to the initial angular momentum and the end-effector velocity.

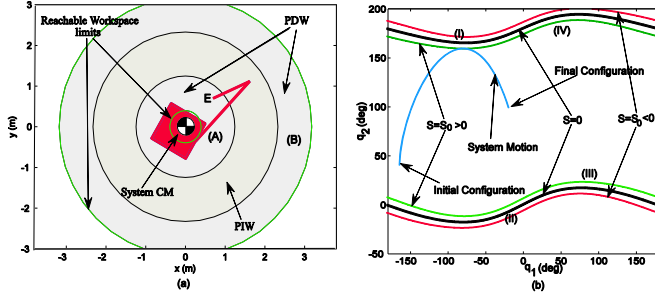


Fig. 4. (a) Path Independent Workspace (PIW) and Path Dependent Workspace (PDW) for a two-dof planar space robot. At E, the manipulator may become singular. (b) Singularity and margin curves and system motion in the joint space avoiding singularities.

As the spacecraft rotates, the rotation matrix  $\mathbf{R}_0(\boldsymbol{\varepsilon}, n)$  in (8) must be updated. The new Euler parameters  $\boldsymbol{\varepsilon}$  and  $n$  are computed according to the following equations [10]:

$$\dot{\boldsymbol{\varepsilon}} = (1/2)[\boldsymbol{\varepsilon}^\times + n\mathbf{I}]^0 \boldsymbol{\omega}_0 \quad (9a)$$

$$\dot{n} = -(1/2)\boldsymbol{\varepsilon}^T \boldsymbol{\omega}_0 \quad (9b)$$

where  $\mathbf{I}$  is the 3x3 unity matrix.

Eq. (8) and (9) can be solved numerically to yield the required joint angles  $\mathbf{q}$  and the resulting spacecraft attitude  $\boldsymbol{\varepsilon}, n$ , so that the end-effector follows the desired path. Then, (3) yields the required joint torques. However, these fail in the presence of a dynamic singularity. Next we propose a novel methodology, that allows path following avoiding the DS. The method is illustrated first for a planar system.

#### IV. SINGULARITY AVOIDANCE

In the previous section, it was mentioned that the path planning in the Cartesian space is constrained by the occurrence of the DS. A point in the PDW may become singular or not, depending on the path the end-effector has followed to reach it. Here, the case of a predefined end-effector path is studied. Then, the manipulator configuration evolution during path-following depends solely on the initial system configuration. If the path is constrained to be in the PIW, all initial configurations are valid. However, if the path has points in the PDW, then it can encounter DS. In this case, the range of initial configurations that guarantee that the end-effector will be able to follow the desired path avoiding any DS, must be found.

To this end, we propose a novel method that determines all valid initial system configurations for following paths in the PDW. The method is illustrated for straight-line paths, and a two-dof planar system with zero angular momentum, see Fig. 3. However, it is applicable to planar and spatial systems with non-zero angular momentum following any path.

For the system in Fig. 3, the end point position is, [9]

$$x_E = ac_{\theta_0} + bc_{\theta_1} + cc_{\theta_2} \quad (10a)$$

$$y_E = as_{\theta_0} + bs_{\theta_1} + cs_{\theta_2} \quad (10b)$$

where  $a, b, c$  are constant length terms, functions of the system mass properties, see Fig. 3b, and  $\theta_i$ ,  $i=0,1,2$  shown in Fig. 3a, with  $c_{\theta_i} = \cos\theta_i$ ,  $s_{\theta_i} = \sin\theta_i$ . The end-effector linear velocity can be found by differentiating (10).

Assuming zero initial momentum, (8) take the form,

$$\dot{\theta}_0 = \frac{\dot{x}_E(bD_2c_{\theta_1} - cD_1c_{\theta_2}) + \dot{y}_E(bD_2s_{\theta_1} - cD_1s_{\theta_2})}{S(q_1, q_2)} \quad (11a)$$

$$\dot{q}_1 = \frac{\dot{x}_E[-D_2(ac_{\theta_0} + bc_{\theta_1}) + c(D_0 + D_1)c_{\theta_2}] + \dot{y}_E[-D_2(as_{\theta_0} + bs_{\theta_1}) + c(D_0 + D_1)s_{\theta_2}]}{S(q_1, q_2)} \quad (11b)$$

$$\dot{q}_2 = \frac{\dot{x}_E[a(D_1 + D_2)c_{\theta_0} - D_0(bc_{\theta_1} + cc_{\theta_2})] + \dot{y}_E[a(D_1 + D_2)s_{\theta_0} - D_0(bs_{\theta_1} + cs_{\theta_2})]}{S(q_1, q_2)} \quad (11c)$$

where  $D_i$ ,  $i=0,1,2$  are given in [6] and

$$S(q_1, q_2) = abD_2s_1 + bcD_0s_2 - acD_1s_{12} = k_0(q_1) + k_1(q_1)s_2 + k_2(q_1)c_2 \quad (12)$$

with  $s_i = \sin q_i$ ,  $c_i = \cos q_i$ ,  $s_{ij} = \sin(q_i + q_j)$ . The parameters  $k_i(q_1)$ ,  $i=0,1,2$  are given by:

$$k_0(q_1) = (2aba_{22} - c(aa_{21} + ba_{02}))s_1 / 2 \quad (13a)$$

$$k_1(q_1) = -(aba_{02} + aca_{01} - 2bca_{00}) / 2 + c(-aa_{11} + ba_{01})c_1 + a(ba_{02} - ca_{01})\cos(2q_1) / 2 \quad (13b)$$

$$k_2(q_1) = a(ba_{21} - ca_{11})s_1 + a(ba_{02} - ca_{01})\sin(2q_1) / 2 \quad (13c)$$

where the coefficients  $a_{ij}$  are given in Appendix A.

When  $S=0$ , the manipulator becomes dynamically singular. The function  $S$  is trigonometric and is bounded by  $S_{\max} = \max S(q_1, q_2)$  and  $S_{\min} = \min S(q_1, q_2)$ ,  $q_1, q_2 \in [0, 2\pi]$ . Using (12), one can find that the equation  $S=S^*$ ,  $S^* \in [S_{\min}, S_{\max}]$  yields two solutions:

$$q_2 = \arcsin[(S^* - k_0)\cos\varphi / k_1] - \varphi \quad (14a)$$

$$q_2 = \pi - \arcsin[(S^* - k_0)\cos\varphi / k_1] - \varphi \quad (14b)$$

where,

$$\varphi = \arctan[k_2 / k_1] \quad (14c)$$

Note that Eqs. (14) with  $S^*=0$ , yield the singularity curves (I) and (II) in Fig. 4b and their locations define the PDW (B) and (A) respectively in Fig. 4a. As the end-effector follows the desired path, the manipulator configuration traces a curve in the  $q_2 - q_1$  space. The manipulator will be singular, if this curve intersects curves (I) or (II). To avoid singularities, a safety margin  $S_0 \in [S_{\min}, 0) \cup (0, S_{\max}]$  is defined. Then, a sufficient condition to avoid singularities is that the end-effector traced curve and the margin curve  $S(q_1, q_2) = S_0 \neq 0$ , (curves (III) and (IV) in Fig. 4b), have only one intersection point or, equivalently, that they have a common tangent.

At a point  $(q_1, q_2)$ , the configuration curve slope is:

$$\lambda_1 = \frac{dq_2}{dq_1} = \frac{\dot{q}_2}{\dot{q}_1} \quad (15)$$

The desired end-effector path and corresponding rates are:

$$y_E = K x_E + L \quad (16a)$$

$$\dot{y}_E = K \dot{x}_E \quad (16b)$$

Using (16b), (11b) – (11c) take the form:

$$\dot{q}_1 = \frac{\dot{x}_E}{S} g_1(\theta_0, q_1, q_2), \dot{q}_2 = \frac{\dot{x}_E}{S} g_2(\theta_0, q_1, q_2) \quad (17)$$

where,

$$g_1 = (-D_2(ac_{\theta_0} + bc_{\theta_1}) + c(D_0 + D_1)c_{\theta_2}) + K(-D_2(as_{\theta_0} + bs_{\theta_1}) + c(D_0 + D_1)s_{\theta_2}) \quad (18a)$$

$$g_2 = (a(D_1 + D_2)c_{\theta_0} - D_0(bc_{\theta_1} + cc_{\theta_2})) + K(a(D_1 + D_2)s_{\theta_0} - D_0(bs_{\theta_1} + cs_{\theta_2})) \quad (18b)$$

Using (15) and (17), the slope of the configuration curve is written as,

$$\lambda_1 = \frac{dq_2}{dq_1} = \frac{\dot{q}_2}{\dot{q}_1} = \frac{g_2(\theta_0, q_1, q_2)}{g_1(\theta_0, q_1, q_2)} = G_1(\theta_0, q_1, q_2) \quad (19)$$

The slope of the margin curve

$$S(q_1, q_2) = S_0 \quad (20)$$

at a point  $(q_1, q_2)$  is given by:

$$\lambda_2 = \frac{dq_2}{dq_1} = \frac{\dot{q}_2}{\dot{q}_1} = -\frac{\frac{\partial S(q_1, q_2)}{\partial q_1}}{\frac{\partial S(q_1, q_2)}{\partial q_2}} = G_2(q_1, q_2) \quad (21)$$

If the two curves have a common tangent, then,

$$\lambda_1 = \lambda_2 \Rightarrow G_1(\theta_0, q_1, q_2) = G_2(q_1, q_2) \quad (22)$$

In addition (10) and (16a) give:

$$as_{\theta_0} + bs_{\theta_1} + cs_{\theta_2} = K(ac_{\theta_0} + bc_{\theta_1} + cc_{\theta_2}) + L \quad (23)$$

Eqs. (20), (22) and (23) can be solved to yield  $\theta_0, q_1, q_2$ . More specifically, (20) can be solved analytically and give  $q_2$  as a function of  $q_1$ , see (14). Eq. (23) is equivalent to,

$$(h_1 + K h_2)s_{\theta_0} + (h_2 - K h_1)c_{\theta_0} = L \quad (24)$$

where,

$$h_1 = a + bc_1 + cc_{12}, h_2 = bs_1 + cs_{12} \quad (25)$$

Using trigonometric transformations, one finally gets,

$$(L + (h_2 - Kh_1))x^2 + 2(h_1 + Kh_2)x + L - (h_2 - Kh_1) = 0 \quad (26)$$

where,

$$x = \tan(\theta_0/2) \quad (27)$$

Eqs. (26), (27) yield two solutions for  $\theta_0$  at the tangent point, as a function of  $q_1, q_2$ . Due to (20),  $q_2$  is a function of  $q_1$ , and therefore, both  $\theta_0$  and  $q_2$  at the common tangent point are functions of  $q_1$ . For a range of  $q_1$ , the configurations that satisfy (22) are computed. Note that some of the solutions must be rejected (e.g. they belong out of the desired

path limits). Then using these solutions as initial conditions and solving (11) backwards to the initial point of the path given by (16b), yields the desired initial system configuration that bounds the range of feasible configurations.

**Example 1:** To illustrate the developed method, the planar manipulator in Fig. 3 with parameters in Table I is employed. The end-effector is driven from point A=(2.0,0) m to point B=(-1.0,1.5) m following a straight-line path, lying in the PDW. Hence, the manipulator may become singular.

Table I. Parameters of the system shown in Fig. 3.

Body	$l_i$ (m)	$r_i$ (m)	$m_i$ (Kg)	$I$ (Kg m <sup>2</sup> )
0	0.5	0.5	400	66.67
1	1.0	1.0	40	3.33
2	0.5	0.5	30	2.50

Next, the method described in this section is employed to find the appropriate initial configurations that guarantee that no DS will be encountered. The maximum value of  $S$  in (12) is  $S_{\max} \approx 150$ . We choose  $S_0 = 5$  ( $S_0 \approx 3.3\% S_{\max}$ ). Then (20), (22) and (23) give the following configurations at which the configuration curve is tangent to the margin curve  $S = S_0$ :

$$(\theta_0, q_1, q_2)^T = (2.028, -0.386, 2.982)^T \text{ rad}$$

$$(\theta_0, q_1, q_2)^T = (0.550, -0.585, 2.932)^T \text{ rad}$$

$$(\theta_0, q_1, q_2)^T = (2.377, -1.030, 2.864)^T \text{ rad}$$

Using these solutions as initial conditions and solving (11) backwards to the initial point of the path, one gets the desired initial spacecraft orientation. The first solution yields no valid result, while the other two yield the limits for the inadmissible range of attitudes, i.e.  $\theta_{0,1}^m = 80.4^\circ$  and  $\theta_{0,2}^m = 270.9^\circ$ .

Fig. 5 and 6 show the system motion when the initial base orientation is  $\theta_0^m = 150^\circ$ , and  $\theta_0^m = 10^\circ$ , respectively. In the first case, the initial attitude is between the boundaries computed above and therefore the desired motion is not feasible (the manipulator becomes singular at point C). In the second case, the chosen initial base orientation permits the end-effector to follow the desired path. Figs. 7(a) and 7(b) show the resulting trajectories and their rates respectively.

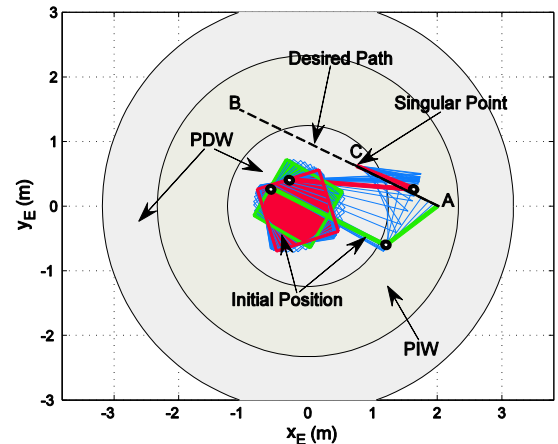


Fig. 5. Motion animation of space manipulator motion with  $\theta_0^m = 150^\circ$ .

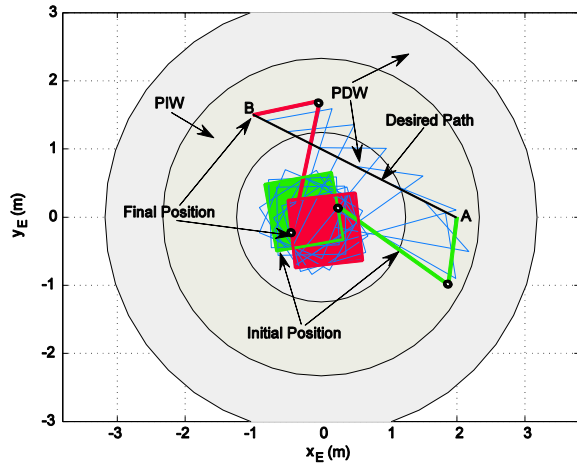


Fig. 6. Motion animation of space manipulator motion with  $\theta_0^{in} = 10^0$ .

The above analysis concludes that the allowable initial base orientations should range below  $\theta_{0,1}^{in}$  or above  $\theta_{0,2}^{in}$ . This range can be increased if a smaller value for  $S_0$  is selected.

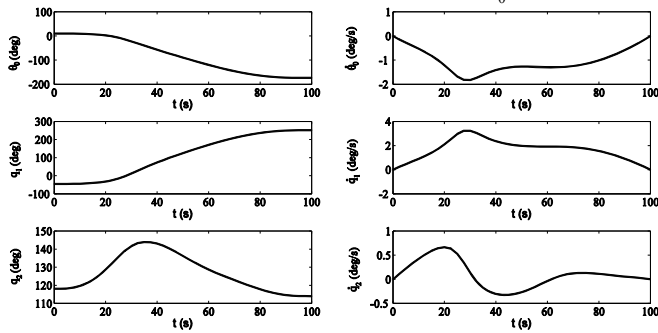


Fig. 7. For the motion in Fig. 9, (a) Spacecraft attitude and joint angle trajectories (b) Spacecraft attitude and joint angle rates.

## V. EXTENSION TO SPATIAL SYSTEMS

The method described in Section IV is extended to spatial systems such as the free-floating space manipulator shown in Fig. 2. As in the planar case, the end-effector desired path is a straight-line in the Cartesian workspace of the system.

The end-effector position is a function of the manipulator configuration and the spacecraft attitude described by the Euler parameters, [9]:

$$\mathbf{r}_E = \begin{bmatrix} x_E & y_E & z_E \end{bmatrix}^T = f(\mathbf{e}, \mathbf{n}, \mathbf{q}) \quad (28)$$

The desired end-effector trajectory is described by:

$$y_E = K_1 x_E + L_1 \quad (29a)$$

$$z_E = K_2 x_E + L_2 \quad (29b)$$

where:

$$x_E = s(t) \quad (30)$$

The displacement  $s(t)$  along the path is given by:

$$s(t) = a_0 + a_1 t + a_2 t^2 + a_3 t^3 + a_4 t^4 + a_5 t^5, \quad 0 \leq t \leq t_{fin} \quad (31)$$

Then, the end-effector velocity is simply:

$$\dot{\mathbf{r}}_E = \begin{bmatrix} \dot{s} & K_1 \dot{s} & K_2 \dot{s} \end{bmatrix}^T \quad (32)$$

As the end-effector moves, the manipulator configuration traces a configuration space curve, with tangent vector  $\mathbf{c}$ ,

$$\mathbf{c} = \begin{bmatrix} \dot{q}_1 & \dot{q}_2 & \dot{q}_3 \end{bmatrix}^T \quad (33)$$

For this system,  $\det(\mathbf{S}) = S_0$  defines a surface in the configuration space. It can be shown that the major singularity surface is described by equation of the form:

$$S = f_0(q_2) + f_1(q_2)s_3 + f_2(q_2)c_3 \quad (34)$$

The normal vector  $\mathbf{n}$  of this surface is given by,

$$\mathbf{n} = \begin{bmatrix} \partial S / \partial q_1 & \partial S / \partial q_2 & \partial S / \partial q_3 \end{bmatrix}^T \quad (35)$$

To avoid reaching a DS, the curve defined by (33) must not intersect the surface defined by (34). At the limit, the curve and the surface must just touch at a point in the configuration space. At that point,  $\mathbf{c}$  and  $\mathbf{n}$  will be normal. Therefore we require that:

$$\dot{q}_1 \partial S / \partial q_1 + \dot{q}_2 \partial S / \partial q_2 + \dot{q}_3 \partial S / \partial q_3 = 0 \quad (36)$$

This condition will be used to find admissible orientations that will not lead to DS, as explained next via an example.

**Example 2:** The spatial manipulator shown in Fig. 2 is employed here. The system parameters are given in Table II. The end-effector is driven from point  $A = (1, 0, 0)m$  to point  $B = (-0.5, 0.8, 0.3317)m$  following a straight-line path, lying in the PDW, with  $t_{fin} = 200s$ . Hence, the manipulator may become singular at some point.

If the initial spacecraft attitude is random, for example if it is given by  $\mathbf{e}_0 = [0.2, 0.5, 0.3]^T$ ,  $n_0 = -0.7874$ , the manipulator becomes singular at  $C = (0.1576, 0.4546, 0.1885)m$ . Fig. 8 shows the initial and singular manipulator configurations.

Table II. Parameters of the system shown in Fig. 2.

Body	$l_i$ (m)	$r_i$ (m)	$m_i$ (kg)	$I_{xx}$ (kg m <sup>2</sup> )	$I_{yy}$ (kg m <sup>2</sup> )	$I_{zz}$ (kg m <sup>2</sup> )
0	-	$[0, 0, 0.5]^T$	400	66.67	66.67	66.67
1	0	0	0	0	0	0
2	0.5	0.5	40	0.001	2.5	2.5
3	0.5	0.5	30	0.001	7.5	1.7

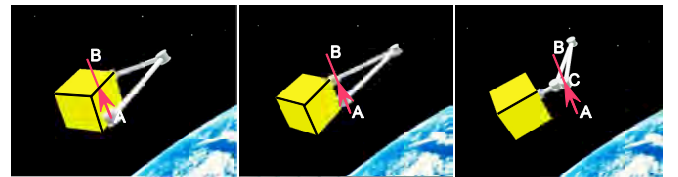


Fig. 8. System motion snapshots. The system becomes singular at point C.

Next, the appropriate initial configurations that guarantee that no DS will be encountered are computed. For increased safety margins,  $S_0 = -5$  is chosen. For a range of  $q_1$  and  $q_2$ , (34) yields the corresponding angle  $q_3$ . Then (28), (29) and (36) give the corresponding spacecraft attitude at which the configuration curve is tangent to the margin surface  $S = S_0$ . One solution is:

$$[q_1, q_2, q_3]^T = [0.1, 2.3, -2.9417]^T \text{ rad}$$

$$[e_1, e_2, e_3, n]^T = [0.0697, -0.4808, -0.3066, -0.8186]^T$$

Using this solution as the initial system configuration and solving (8) backwards to the initial point of the path given by (32), one gets a desired initial spacecraft orientation,

$$[e_1, e_2, e_3, n]^T = [0.0431, -0.3657, -0.3598, -0.8573]^T$$

The initial configuration  $\mathbf{q}$  is found by solving the inverse kinematics problem. The required joint trajectories are computed using (8), (9) and (32). Fig. 9 shows system motion snapshots. The end-effector trajectories are shown in Fig. 10(a), while Fig. 10(b) and (c) show the trajectories of the configuration variables and the spacecraft attitude expressed by  $x$ - $y$ - $z$  Euler angles respectively. Fig. 10(d) and (e) show the robot joint rates and the spacecraft angular velocity expressed in the inertial frame. It can be seen that all trajectories are smooth throughout the motion. The joint torques in Fig. 9 are computed using (3) and shown in Fig. 10(f). The required torques are small and smooth, guaranteeing task feasibility.

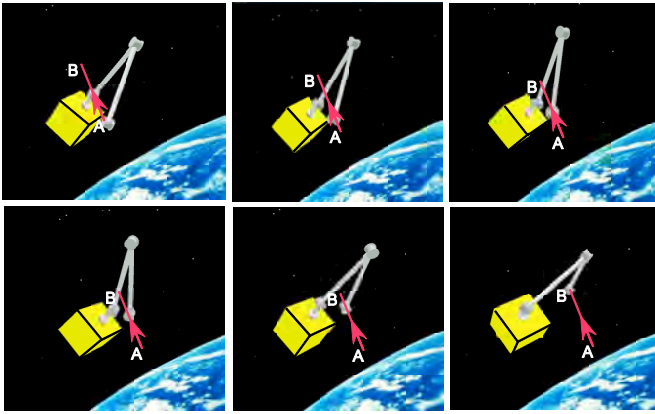


Fig. 9. System snapshots. The end-effector follows the path from A to B without encountering dynamic singularities.

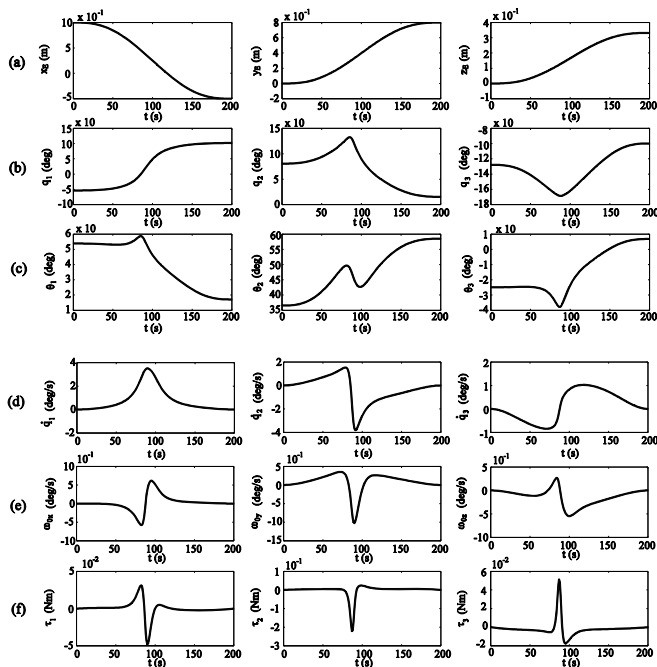


Fig. 10. (a) End-effector position trajectory, (b) Joint angle trajectories, (c) Spacecraft attitude trajectories ( $x$ - $y$ - $z$  Euler angles). (d) Joint angles rates, (e) Spacecraft angular velocity. (f) Manipulator joint torques.

## VI. CONCLUSIONS

In this paper, the Cartesian space path planning of free-floating space robots in the presence of Dynamic Singularities was studied. The locations of the DS in the workspace are path dependent and complicate path planning. It was shown that its workspace is restricted due to the existence of the DS. Next, a path planning technique allowing the end-effector to follow a desired path avoiding DS was developed. Since the path is predefined, the method yields the appropriate initial system configuration range that avoids dynamical singular configurations during the motion. Thus, the entire system workspace can be used. The proposed method was applied to a two-dof planar system with zero angular momentum whose end-effector was commanded to follow a straight-line path and then was extended to a 3-dof spatial system. The method was illustrated by two examples.

## REFERENCES

- [1] Papadopoulos, E., Dubowsky, S., "Dynamic Singularities in the Control of Free-Floating Space Manipulators," *ASME Journal of Dynamic Systems, Measurement and Control*, Vol. 115, No. 1, 1993, pp. 44-52.
- [2] Franch, J., Agrawal, S., Fattah, A., "Design of Differentially Flat Planar Space Robots: A Step Forward in Their Planning and Control," *IEEE/RSJ Intl. Conf. On Intelligent Robots and Systems (IROS'03)*, Las Vegas, Nevada, Oct. 2003, pp. 3053-3058.
- [3] Agrawal, S., Pathak, K., Franch, J., Lampariello, R., and Hirzinger, G., "A Differentially Flat Open-Chain Space Robot with Arbitrarily Joint Axes and Two Momentum Wheels at the Base," *IEEE Trans. on Automatic Control*, Vol. 54, No. 9, Sept. 2009, pp. 2185-2191.
- [4] Nenchev, D., Umetani, Y., and Yoshida, K., "Analysis of a Redundant Free-Flying Spacecraft/Manipulator System," *IEEE Transactions on Robotics and Automation*, Vol. 8, No. 1, February 1992, pp. 1-6.
- [5] Tortopidis, I., and Papadopoulos, E., "On Point-to-Point Motion Planning for Underactuated Space Manipulator Systems," *Robotics and Autonomous Systems*, Vol. 55, No. 2, 2007, pp. 122-131.
- [6] Papadopoulos, E., "Path Planning for Space Manipulators Exhibiting Nonholonomic Behavior," *IEEE/RSJ Intl. Conf. On Intelligent Robots and Systems (IROS'92)*, Raleigh, NC, July 7-10, 1992, pp. 669-675.
- [7] Xu, W., Liang, B., Li, C., Liu, Y., and Xu, Y., "Autonomous Target Capturing of Free-floating Space Robot: Theory and Experiments," *Robotica*, Vol. 27, 2008, pp. 425-445.
- [8] Umetani, Y., Yoshida, K., "Resolved Motion Rate Control of Space Manipulators with Generalized Jacobian Matrix," *IEEE Transactions on Robotics and Automation*, Vol. 5, No. 3, June 1989, pp. 303-314.
- [9] Nanos, K., and Papadopoulos, E., "On the Use of Free-floating Space Robots in the Presence of Angular Momentum," *Intelligent Service Robotics, Sp. Issue on Space Robotics*, Vol. 4, No. 1, 2011, pp. 3-15.
- [10] Hughes, C.P., *Spacecraft Attitude Dynamics*, Wiley, New York, 1986.

## APPENDIX A

The parameters in (13) are given below.

$$a_{00} = I_0 + m_0 (m_1 + m_2) r_0^2 / M \quad (A1)$$

$$a_{01} = m_0 r_0 (l_1 (m_1 + m_2) + r_1 m_2) / M \quad (A2)$$

$$a_{02} = m_0 m_2 r_0 l_2 / M \quad (A3)$$

$$a_{11} = I_1 + (m_0 m_1 l_1^2 + m_1 m_2 r_1^2 + m_0 m_2 (l_1 + r_1)^2) / M \quad (A4)$$

$$a_{21} = m_2 l_2 (m_1 r_1 + m_0 (l_1 + r_1)) / M \quad (A5)$$

$$a_{22} = I_2 + m_2 (m_0 + m_1) l_2^2 / M \quad (A6)$$

$$M = m_0 + m_1 + m_2 \quad (A7)$$